Reprinted from
THE PHYSICS OF FLUIDS VOLUME 12, NUMBER 10 OCTOBER 1969
Printed in U.S.A.

Transverse Kelvin–Helmholtz Instability in a Rotating Plasma

GERALD I. KENT*
Systems, Science and Software, La Jolla, California
NORMAN C. JEN
City College of the City University of New York, New York
AND
FRANCIS F. CHEN
Princeton University, Princeton, New Jersey
(Received 10 March 1969)

In thermally ionized alkali-metal plasmas (Q machines), two types of low-frequency oscillations are found: the usual drift wave localized to the region of large-density gradient, and a higher-frequency wave localized to the region of the radial boundary. The latter "edge" oscillation is shown to be a Kelvin–Helmholtz instability driven by the large shear in plasma rotational velocity at the boundary. An analytic solution of the finite-Larmor-radius dispersion equation for the unstable wave is found by making the simplifying assumption that the rotational velocity jumps discontinuously. The results agree reasonably well with experimental measurements.

I. INTRODUCTION

In recent years there has been considerable work on thermally ionized alkali-metal plasma generators (Q machines[1]) concerning universal instabilities, or drift waves. There is, however, another type of low-frequency oscillation which often arises spontaneously in such plasmas; and we suspect that in early work on universal instabilities the two types of oscillations were confused. When the magnetic field is sufficiently high, the two oscillations can be distinguished by their localization in space, as illustrated in Fig. 1. The amplitude of drift waves is peaked in the region of large density gradient, while the other oscillation, always at a higher frequency, is peaked in the region of large electric field near the aperture limiter. The present work is an experimental study of the latter phenomenon, which we shall call the edge oscillation, and its explanation in terms of the Kelvin–Helmholtz effect.

In hydrodynamics it is well known[2] that a fluid with a gradient in mass flow velocity is subject to the Kelvin–Helmholtz instability. That this also occurs in a plasma when the flow is along the magnetic field **B** has been shown by D'Angelo and von Goeler,[3] but so far this instability has not been reported for flow across **B**. In Fig. 1 it is seen that the edge oscillation occurs in a region where the plasma potential takes a large jump (because of the difference in work function between the emitting hot plate and the cool aperture limiter), and hence a region where there is a large gradient in plasma flow across **B**. One, therefore, suspects that either the large $\mathbf{E}\times\mathbf{B}$ azimuthal rotation velocity or its gradient is connected with the instability. The difficulty is that the gradient scale lengths are not large compared with the ion Larmor radius, and, therefore, ordinary fluid equations for the plasma would not be valid. Fortunately, an analysis of this problem including finite-Larmor-radius effects already exists in the literature. Figure 2 shows that the observed wave travels in the direction of $\mathbf{E}\times\mathbf{B}$ but at a speed intermediate between the electron diamagnetic drift and the maximum $\mathbf{E}\times\mathbf{B}$ drift. The transverse Kelvin–Helmholtz instability is the only one we have been able to find which predicts a frequency in this range.

II. EXPERIMENT

The measurements were carried out in the single-ended Q machine shown in Fig. 3. The hot plate was heated by electron bombardment to temperatures of order 2000–2400°K. A beam of neutral potassium atoms from an oven was directed at the center of the plate by either a single nozzle or an array of three nozzles set in an annular manifold. The atoms are ionized by contact with the tungsten plate. The radius of the plasma was set at about 1 cm by a grounded aperture limiter. The plasma was terminated by a large cold plate biased to reflect electrons. The length L of the plasma column could be varied up to 100 cm, but most measurements were made with $L \approx 50$ cm, in which length the B field was uniform to $\pm 2\%$. The base pressure

* Based on a doctoral dissertation, City University of New York.
[1] N. Rynn, Rev. Sci. Instr. 35, 40 (1964).
[2] S. Chandrasekhar, *Hydrodynamic and Hydromagnetic Stability* (Oxford University Press, London, 1961), Chap. XI.
[3] N. D'Angelo and S. von Goeler, Phys. Fluids 9, 309 (1966).

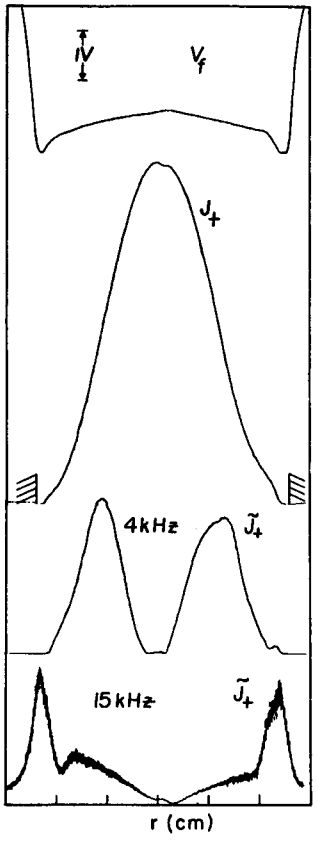

FIG. 1. Radial profiles of plasma potential, plasma density, drift wave amplitude, and edge oscillation amplitude in a double-ended potassium Q machine at about 2 kG. These quantities were approximated by the floating potential V_f of and ion saturation current J_+ to a Langmuir probe. The location of the aperture limiter is shown on the second curve. The last two curves required frequency selection with a Tektronix 1L5 spectrum analyzer. The ion Larmor radius was about 2 mm. These data were taken at the Princeton Plasma Physics Laboratory.

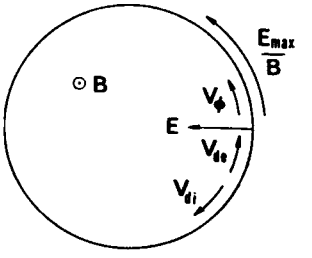

FIG. 2. Relative directions and magnitudes of the observed velocity $v\phi$ and the various drift velocities in the plasma.

was $< 2 \times 10^{-6}$ Torr, and the stainless-steel vacuum chamber walls were water cooled to keep the potassium vapor pressure below 10^{-8} Torr.

Three Langmuir probes were used for detection of the instability. Each had a 0.22-mm-diam tungsten tip 1-mm long and was coaxially shielded inside a ceramic tube of 1.4 mm o.d. One probe could be moved only radially; a second could also be rotated on an offset shaft to change azimuth; and a third could be moved along the magnetic field. Plasma density was measured by saturation ion current using the method of Chen *et al.*[4] Fluctuations in ion current were detected by a 1-kΩ terminating resistor and a Tektronix Type 1A7 preamplifier. Measurements of the probe characteristic showed an electron temperature consistent with the hot plate temperature ($kT_e \approx 0.2$ eV). Fluctuations in floating potential were measured by the method of capacitance neutralization.[5] Frequencies were measured with an oscilloscope and a spectrum analyzer.

Edge oscillations were observed for densities between 5×10^8 and 5×10^{10} cm^{-3}, and for B between 500 and 5200 G. Beyond these limits the density profile deteriorated, so that no clean measurements could be made. Figure 4 shows typical frequency spectra. At low B, the spectrum consists of a fundamental and its harmonics. At high B, the spectrum is broad with an identifiable peak. Typical density

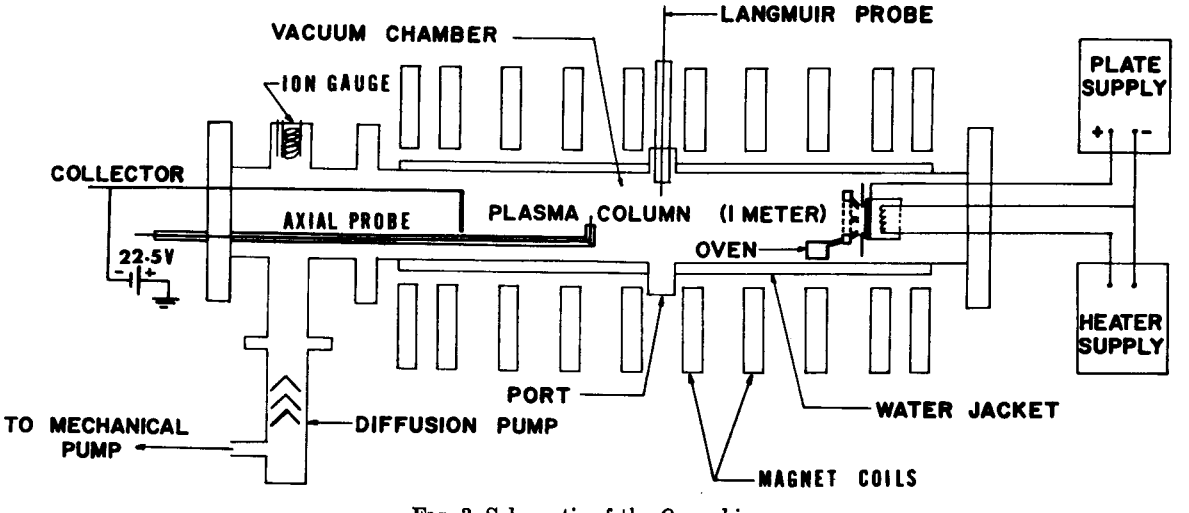

FIG. 3. Schematic of the Q machine.

[4] F. F. Chen, C. Etievant, and D. Mosher, Phys. Fluids 11, 811 (1968).
[5] F. F. Chen, in *Proceedings of the Conference on Physics of Quiescent Plasmas* (Euratom-C.N.E.N., Frascati, Italy, 1967), Pt. II, p. 563.

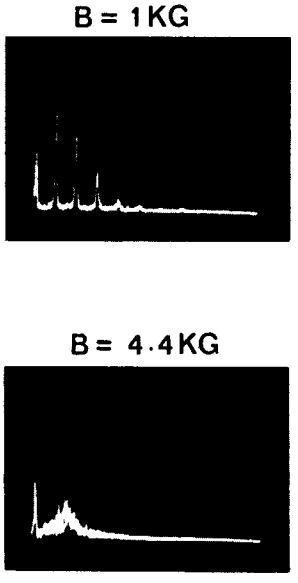

FIG. 4. Typical frequency spectra of edge oscillations at low and high magnetic fields. The leftmost marker is at 0 frequency, and the abscissa is 10 kHz/div. The vertical scale is linear.

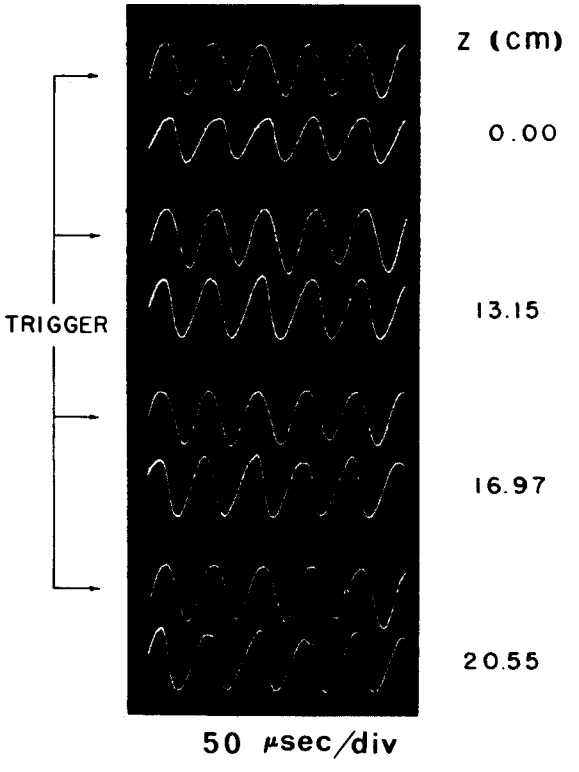

FIG. 6. Measurement of $k_\parallel$. The top trace in each picture is a reference signal from a stationary probe. The bottom trace is the signal from a probe moved along z with r and θ kept constant. The point $z = 0$ is approximately at the midplane of the column, and the probe was moved towards the cold plate.

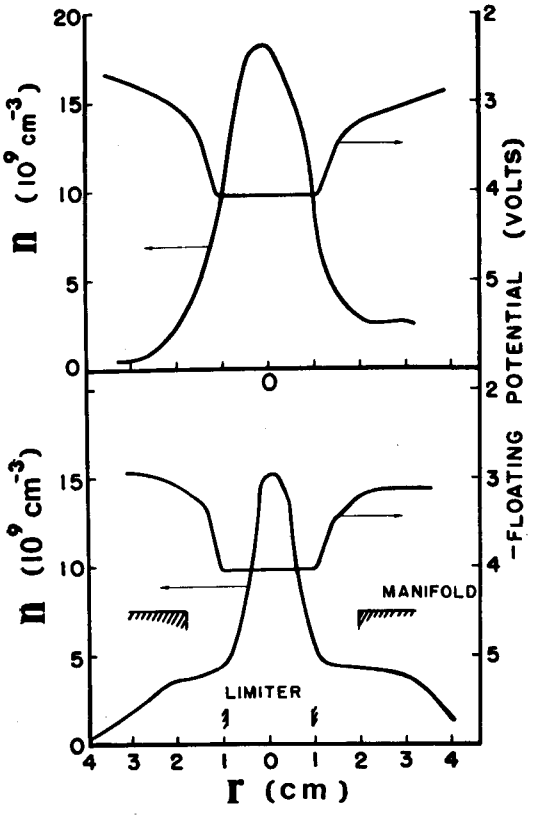

FIG. 5. Typical density and potential profiles with (bottom) and without (top) the oven manifold.

and potential profiles are shown in Fig. 5. Note that the density profile could be changed by altering the diameter of the aperture limiter or removing the oven manifold. However, the nature of the oscillations was not changed, and in any case the measured dc profiles were used to compute the theoretical frequencies. Tests with different types of aperture limiters (disks placed in front of the hot plate or flush with the hot plate, or a tubular limiter) showed no effect on the oscillations other than what would be expected from a change in plasma radius. The potential profiles show that E_r is practically zero in the plasma. This is because the radial temperature gradient in the hot plate nearly cancels the electric field associated with the density gradient.[6] The large E_r at the edge of the column is due to the change from an electron sheath in the interior region to an ion sheath in the exterior region, together with the change in contact potentials. The rise in potential at large radius is probably due to the fact that ions can migrate across **B** faster than electrons.

Since it is of primary importance to the theory

[6] F. F. Chen, Phys. Fluids 9, 2534 (1966).

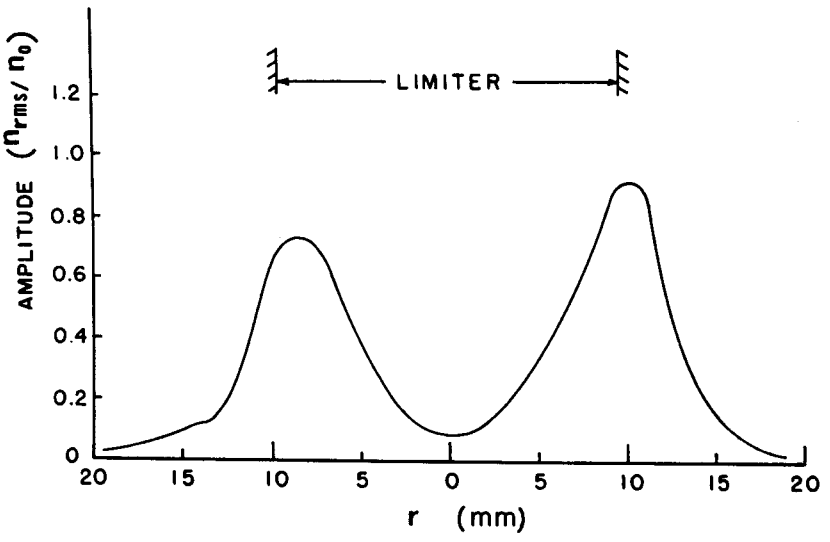

FIG. 7. Radial profile of wave amplitude, as measured by the perturbed density n_1 divided by the local dc density n_0.

whether $k_\parallel$ is zero or finite, we took pains to measure $k_\parallel$ with a probe movable along **B** and rotatable about an axis near the bottom of the vacuum chamber. By choosing a point on the steep part of the density profile and measuring the ion current, it was possible to reposition the probe at the same radius each time the position z along **B** was changed. To keep θ constant, we relied on accurate optical alignment of the vacuum chamber with the magnetic field coil system. Figure 6 shows a measurement of $k_\parallel$. From the change in phase shift of the movable probe signal relative to the fixed probe signal, we can place an upper limit of 6×10^{-3} cm^{-1} on $k_\parallel$. This would give a wavelength $\lambda_\parallel = 20L$. Because of the smallness of $k_\parallel$, a small error in azimuthal probe position would greatly affect the results. We estimate the possible error in $k_\parallel$ to be $\approx 10^{-2}$ cm^{-1}. This gives $\lambda_\parallel \geq 8L$. However, if the wave is a standing wave rather than a traveling wave in the z direction, one would expect no phase shift but only an amplitude change with z. From the observed amplitude change we can again place a lower limit of about $8L$ on $\lambda_\parallel$. This indicates a flute mode; drift waves normally have $\lambda_\parallel \approx 2L$. We shall return to this point later.

Further evidence for $k_\parallel = 0$ were provided by two other checks. First, if L is changed by 50%, there is no observable change in frequency or amplitude of the wave. Second, the phase shift between the density fluctuation and the potential fluctuation was found to be $\sim 180°$, rather than $\sim 0°$. As explained by Chen,[7] this indicates a flute, rather than a drift, mode. There is a question of why end-plate damping[8] would not prevent flute instabilities from arising. Apparently, the wave is excited in the region outside the aperture limiter, where there is no thermionic emission, and, therefore, no end-plate damping. Figure 7 shows that the wave amplitude is indeed peaked at the extreme edge of the plasma column.

The azimuthal propagation of the wave was measured by two probes with a variable separation in θ. Figure 8 shows phase shift measurements for the $m = 3$ and $m = 4$ azimuthal modes. We have also measured the radial propagation; there was no measureable phase shift for radial probe separations, indicating a standing wave in the radial direction.

The dependence of wave velocity on magnetic field is shown in Fig. 9, in which the frequency divided by the azimuthal mode number m is plotted against a normalized $|B|$. It is seen that the wave velocity is constant at high **B** and rises at low **B**. This can be understood qualitatively as follows. The wave velocity $\omega/k_\perp$ is proportional to the drift velocity E/B in the "edge" region. If the jump is potential $\Delta\phi$ is constant and the thickness of the transition region scales as the Larmor radius r_L, then we have $\omega/k_\perp \propto E/B \propto \Delta\phi/r_L B$. Since $r_L \propto B^{-1}$, $\omega/k_\perp$ is constant with B. At low fields, however, the Larmor radius becomes comparable to the plasma radius R, and the thickness of the transition region scales as R rather than as r_L. Then, we have $\omega/k_\perp \propto \Delta\phi/RB \propto B^{-1}$. This explains the rise in $\omega/k_\perp$ as **B** is lowered to very small values.

[7] F. F. Chen, Phys. Fluids **8**, 912 (1965).

[8] F. F. Chen, J. Nucl. Energy, Pt. C, **7**, 399 (1965).

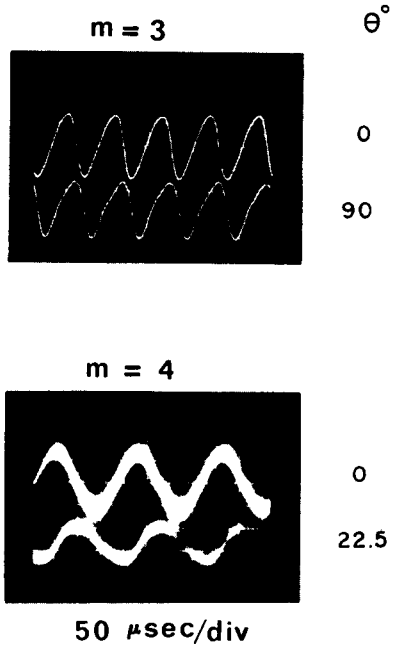

FIG. 8. Example of the measurement of azimuthal mode numbers. The upper picture shows the 90° phase shift produced by an $m = 3$ mode when the probes are separated by 90°. The bottom picture shows the 90° phase shift of an $m = 4$ mode when the probes are separated by $22\frac{1}{2}$°. In the latter case multiple sweeps of the oscilloscope were used to average over the noise.

Figure 10 shows the mode amplitude as a function of B for the $m = 3$, 4, and 5 modes. It is seen that the higher modes successively peak as **B** is increased.

Finally, we have considered the possibility that the waves are excited by shear in $v_\parallel$, as in the work of D'Angelo and von Goeler,[3] rather than by shear in v_θ. This experiment was done with a negative bias on the cold collector plate, so that ions flow only toward the plate both inside and outside the aperture limiter, and there can be no large shear in $v_\parallel$ at the edge. If the negative bias is varied, there is no effect on the oscillations. If the collector plate is made slightly positive relative to the plasma so that some ions are reflected, the wave is still unstable; but the spectrum is modified by instabilities connected with electron flow along **B**. For large positive biases, the latter instabilities mask the edge oscillation.

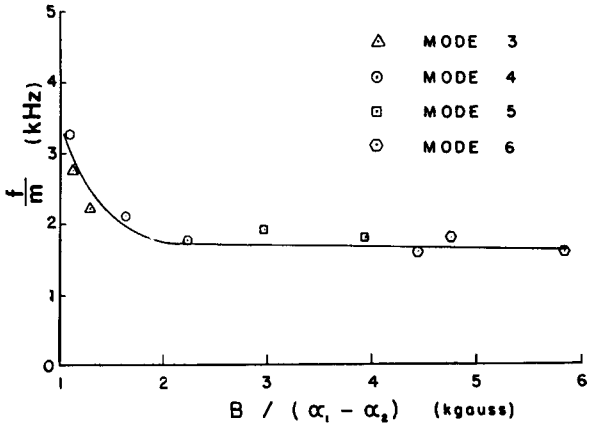

FIG. 9. Wave velocity f/m vs magnetic field B. The abscissa has been scaled by a factor $(\alpha_1 - \alpha_2)^{-1}$ which appears in combination with B in the theory. The factor $\alpha_1 - \alpha_2$ is the fractional change in density in going from the inside region to the outside region.

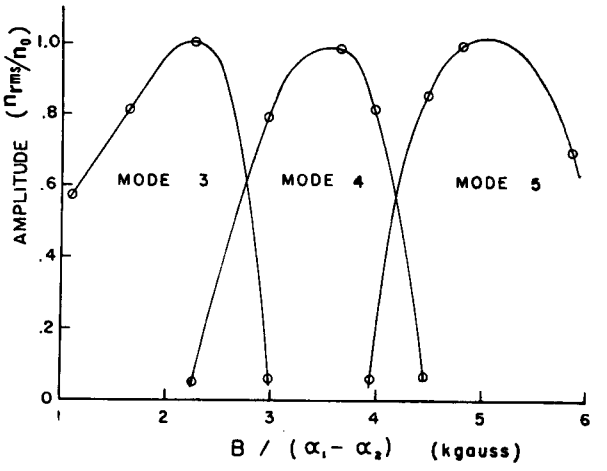

FIG. 10. Wave amplitude n_1/n_0 as a function of $B/(\alpha_1 - \alpha_2)$ (see caption of FIG. 9).

III. THEORY

A. Two-Region Solution

We shall use as our fundamental equation the radial wave equation given by Rosenbluth and Simon[9]

$$(T\psi')' + \left(\frac{1 - m^2}{r^2} T + r^2\omega^2\rho'\right)\psi = 0, \qquad (1)$$

where

$$T \equiv \rho r^3 \bar{\omega}(\bar{\omega} - \omega_{di}), \qquad (2)$$

$$\bar{\omega} \equiv \omega - m\omega_0 \equiv \omega - \frac{m}{r} V_0 = \omega + \frac{m}{r}\frac{E_0}{B}, \qquad (3)$$

$$\omega_{di} \equiv \frac{KT_i}{eB}\frac{m}{r}\frac{\rho'}{\rho}, \qquad \psi \equiv \frac{E_\theta}{\bar{\omega}}, \qquad (4)$$

and the prime denotes $\partial/\partial r$. This equation describes low-frequency flute perturbations of the form $\exp[i(m\theta - \omega t)]$ propagating around an isothermal, cylindrical plasma with an arbitrary density profile $\rho(r)$ and an arbitrary radial electric field

[9] M. N. Rosenbluth and A. Simon, Phys. Fluids **8**, 1300 (1965).

$E_0(r)$ in equilibrium. Equation (1) includes finite-Larmor-radius effects to order $(r_L/R)^2$ and is derivable from fluid equations with collisionless viscosity,[9] from guiding-center equations,[10] or directly from the Vlasov equation.[9] If the ion diamagnetic drift frequency ω_{di} is set equal to zero, one recovers the usual equation for the Kelvin–Helmholtz instability in an ordinary fluid[2] with a velocity distribution $V_0(r)$. The gravitational force has been set equal to zero in Eq. (1), but the last term represents an effective gravitational force due to the centrifugal force.

Analytic solutions of Eq. (1) and complex eigenvalues for ω can be found only for special forms of the functions $\rho(r)$ and $E_0(r)$. In this problem the radial variation of the perturbation is important, and one cannot use a "local" approximation which neglects the radial derivatives. To find a simple solution we have chosen to make the approximation that $\rho(r)$ and $V_0(r)/r$ are constant in each of two regions but make discontinuous jumps at an interface $r = r_s$, as shown in Fig. 11. The reasonability of this approximation will be discussed later.

With this simplification, ω_{di} vanishes and $\tilde{\omega}$ is constant in each region. Within each region, Eqs. (1) and (2) become

$$\psi'' + \frac{3}{r}\psi' + \frac{1 - m^2}{r^2}\psi = 0, \tag{5}$$

$$T = \rho r^3 \tilde{\omega}^2. \tag{6}$$

The solution of Eq. (5) is $\psi = Ar^{-1+m} + Br^{-1-m}$. We now specify $m \geq 1$ without loss of generality and require that ψ be finite at $r = 0$ and vanish at $r = \infty$. Thus, we have

$$\begin{aligned} \psi_1 &= Ar^{-1+m} \quad \text{(interior region)}, \\ \psi_2 &= Br^{-1-m} \quad \text{(exterior region)}. \end{aligned} \tag{7}$$

To connect these solutions at the interface, we follow standard procedure[2] and derive a jump condition by integrating Eq. (1) from $r_s - \epsilon$ to $r_s + \epsilon$ and taking the limit $\epsilon \to 0$. We assume that the Lagrangian displacement ψ/B of a fluid element is continuous across the interface—that is, that there is no separation. Terms in Eq. (1) which do not contain a derivative then disappear, and we have

$$\Delta(T\psi') + [(m^2 - 1)m\tilde{\omega}_s \cdot (KT_i/eB) + r_s^2\omega^2]\,\Delta\rho\,\psi_s = 0, \tag{8}$$

[10] T. E. Stringer and G. Schmidt, Plasma Phys. 9, 53 (1967).

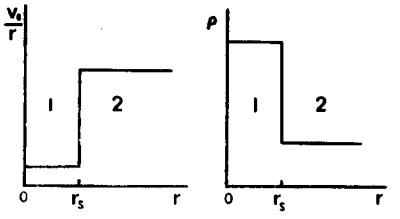

FIG. 11. Form of the zero-order distributions of rotation frequency and density assumed in the two-region solution.

where

$$\psi_s = Ar_s^{-1+m} = Br_s^{-1-m} \tag{9}$$

and

$$\tilde{\omega}_s = \tfrac{1}{2}(\tilde{\omega}_1 + \tilde{\omega}_2), \tag{10}$$

$\tilde{\omega}_1$ and $\tilde{\omega}_2$ being the constant values of $\tilde{\omega}$ in regions 1 and 2, respectively. The jump in $T\psi'$ is computed from Eqs. (6) and (7), and we have

$$(m + 1)\rho_2\tilde{\omega}_2^2 + (m - 1)\rho_1\tilde{\omega}_1^2 - [\omega^2 + 2\gamma m(m^2 - 1)\tilde{\omega}_s](\rho_2 - \rho_1) = 0, \tag{11}$$

where

$$\gamma \equiv (1/2r_s^2)(KT_i/eB). \tag{12}$$

The finite-Larmor-radius effects appear only in the γ term. This term comes from the middle term in Eq. (1), in which T becomes infinite at r_s because ω_{di} contains ρ'. With the use of Eq. (3) and the definitions

$$\alpha_{1,2} \equiv \rho_{1,2}/(\rho_1 + \rho_2), \quad \omega_{1,2} = V_{01,2}/r, \tag{13}$$

Eq. (11) becomes

$$\omega^2 - 2[\alpha_1(m - 1)\omega_1 + \alpha_2(m + 1)\omega_2 + \gamma(m^2 - 1)(\alpha_2 - \alpha_1)]\omega + m(m + 1)\alpha_2\omega_2^2 + m(m - 1)\alpha_1\omega_1^2 - \gamma m(m^2 - 1)(\omega_1 + \omega_2)(\alpha_2 - \alpha_1) = 0. \tag{14}$$

Thus, we have explicit expressions for the frequency and growth rate:

$$\mathrm{Re}\,(\omega) = (m - 1)\alpha_1\omega_1 + (m + 1)\alpha_2\omega_2 + \gamma(m^2 - 1)(\alpha_2 - \alpha_1), \tag{15}$$

$$[\mathrm{Im}\,(\omega)]^2 = -[(m - 1)\alpha_1\omega_1 + (m + 1)\alpha_2\omega_2 + \gamma(m^2 - 1)(\alpha_2 - \alpha_1)]^2 + m(m - 1)\alpha_1\omega_1^2 + m(m + 1)\alpha_2\omega_2^2 + \gamma m(m^2 - 1)(\omega_1 + \omega_2)(\alpha_2 - \alpha_1). \tag{16}$$

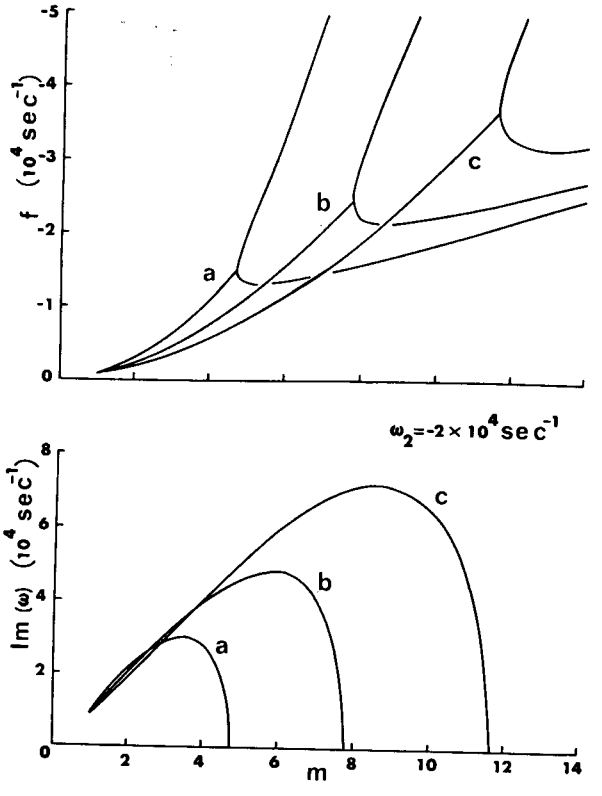

FIG. 12. The two-region solution for frequency f and growth rate Im(ω) as a function of m-number for $\omega_1 = 0$, $\omega_2 = -2 \times 10^4$ sec^{-1}, and $\gamma(\alpha_1 - \alpha_2) = 3750$(a), 2250(b), and 1500(c). Curve c, for instance, corresponds to $\rho_1 = 7\rho_2$, $r_s = 1$ cm, and $B = 5$ kG. Magnetic field increases as one goes from curve (a) to curve (c).

The condition for instability $[\mathrm{Im}\ (\omega)]^2 > 0$ can be rewritten as follows:

$$\alpha_1\alpha_2[(m-1)\omega_1 - (m+1)\omega_2]^2 + (m-1)\alpha_1\omega_1^2 - (m+1)\alpha_2\omega_2^2 > \gamma(m^2-1)(\alpha_2-\alpha_1)^2[\gamma(m^2-1) + m(\omega_2-\omega_1) + 2(\alpha_1\omega_1 - \alpha_2\omega_2)(\alpha_1-\alpha_2)^{-1}]. \quad (17)$$

The physical interpretation of this dispersion relation is clear. The first term in Eq. (17) represents the Kelvin–Helmholtz excitation of the instability. This term is always destabilizing and is essentially proportional to the shear in the zero-order $\mathbf{E}\times\mathbf{B}$ velocity. Note that, as expected, the density in both regions must be finite for this effect to exist. The other two terms on the left-hand side of Eq. (17) represent the net centrifugal force. A "gravitational" instability is excited if the inner region is more dense and/or spins faster than the outer region. In our experiment, $\alpha_1\omega_1^2$ is less than $\alpha_2\omega_2^2$, so that the centrifugal force is actually stabilizing; the destabilizing effect is entirely Kelvin–Helmholtz. The terms on the right-hand side of Eq. (17) depend on γ and represent the finite-Larmor-radius damping of large m-number perturbations. The oscillation frequency, as seen in Eq. (15), is essentially a density-weighted average of the $\mathbf{E}\times\mathbf{B}$ drift velocities in the two regions, modified by the finite-Larmor-radius term in γ.

Typical plots of frequency f and growth rate Im (ω) are shown in Figs. 12 and 13. In Fig. 12, the $\mathbf{E}\times\mathbf{B}$ drift is in such a direction that the finite-Larmor-radius term in Eq. (15) adds to the frequency. Note that the growth rate is sharply cut off at large m numbers, as is normal in finite-Larmor-radius stabilization, that the growth rate peaks at shorter wavelengths as r_L is decreased, and that more modes are simultaneously unstable at higher B fields. Note also that the $m = 1$ mode does not depend on γ, and hence is not affected by finite-Larmor-radius stabilization, as shown long ago by by Rosenbluth *et al.*[11] In Fig. 13, the $\mathbf{E}\times\mathbf{B}$ drift is in such a direction that the finite-Larmor-radius term in Eq. (15) opposes the drift, resulting in very low frequencies. Unfortunately, this is the direction of E_0 in the experiment, and the predicted frequencies are considerably lower than observed. To remedy this, we go to the three-region treatment.

B. Three-Region Solution

In the two-region solution, the region of large electric field (see Fig. 5) is neglected altogether. Since ions spend a finite amount of time in this region, it is clear that the two-region treatment would predict too low a wave velocity. To account for the Doppler shift in the high-field region, we now divide the plasma into three sections, as shown in Fig. 14. Region 2 is now the comparatively thin layer in which E_0 is large.

Proceeding as before, we now have, in place of Eq. (7), the following:

$$\psi_1 = Ar^{m-1}, \quad \psi_2 = Br^{m-1} + Cr^{-m-1}, \quad \psi_3 = Dr^{-m-1}. \quad (18)$$

There are now two jump conditions of the form of Eq. (18), one at r_{23} and one at r_{12}. These yield

$$(C/D)2m\rho_2\bar{\omega}_2^2 = (m-1)\rho_2\bar{\omega}_2^2 + (m+1)\rho_3\bar{\omega}_3^2 - [\omega^2 + m(m^2-1)(KT_i/eB)\cdot(\bar{\omega}_{23}/r_{23}^2)](\rho_3-\rho_2) \equiv W_1, \quad (19)$$

$$(C/A)2m\rho_2\bar{\omega}_2^2 r_{12}^{-2m} = (m-1)\rho_2\bar{\omega}_2^2 - (m-1)\rho_1\bar{\omega}_1^2 + [\omega^2 + m(m^2-1)(KT_i/eB)\cdot(\bar{\omega}_{12}/r_{12}^2)](\rho_2-\rho_1) \equiv W_2. \quad (20)$$

[11] M. N. Rosenbluth, N. A. Krall, and N. Rostoker, Nucl. Fusion Suppl., Pt. 1, 143 (1962).

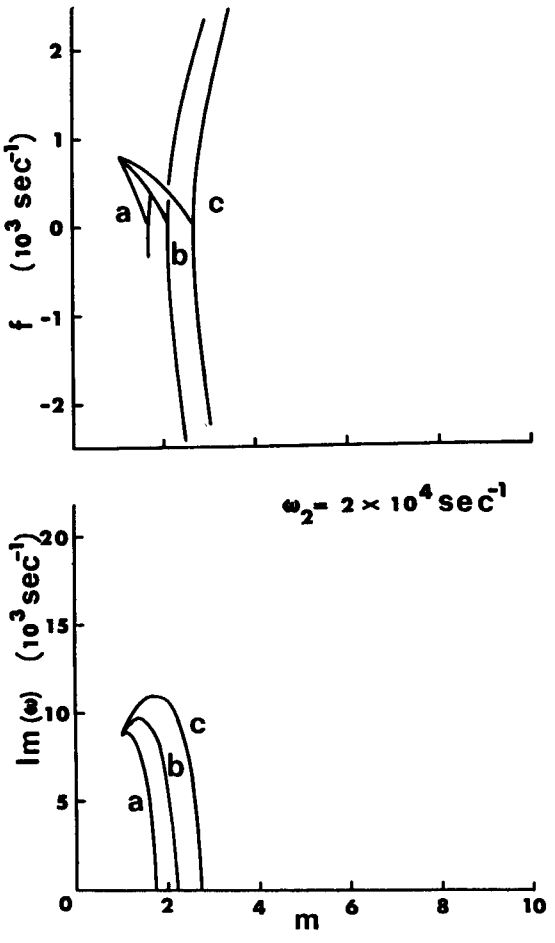

FIG. 13. Dispersion curves for $\omega_2 = 2 \times 10^4$ sec^{-1}. Other parameters as in FIG. 12.

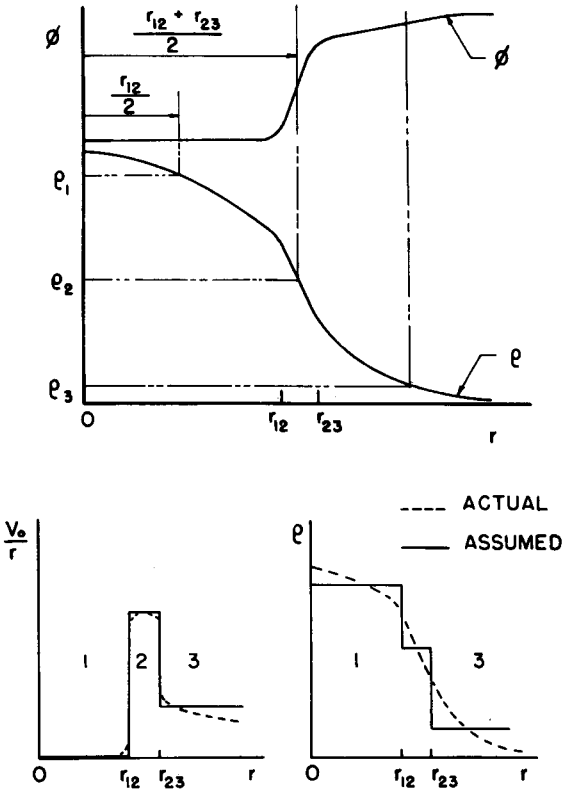

FIG. 14. Form of the zero-order distributions of V_0/r and ρ assumed in the three-region solution. The upper diagram illustrates how a measured set of profiles would be divided into three regions of constant V_0/r and ρ.

In Eq. (19), the coefficient B has been eliminated by the condition $\psi_2 = \psi_3$ at r_{23}. Similarly, B has been eliminated from Eq. (20) by $\psi_1 = \psi_2$ at r_{12}. These two conditions on B yield a third equation

$$D/C = (A/C)r_{23}^{2m} + 1 - (r_{23}/r_{12})^{2m}. \quad (21)$$

The coefficients C/D and C/A can now be eliminated from Eqs. (19)–(21) to give the equation

$$W_2 - W_1 = \epsilon W_1(1 - W_2 W_0^{-1}), \quad (22)$$

where $W_0 \equiv 2m\rho_2\bar{\omega}_2^2$, $\epsilon \equiv (r_{23}/r_{12})^{2m} - 1$, and W_1 and W_2 are defined above.

Equation (22) is a quartic equation for ω. To reduce it to a quadratic, we make use of the approximation $\omega_2 \gg \omega, \omega_1, \omega_3, \omega_{di}$. On the right-hand side of Eq. (22), which is multiplied by the small quantity ϵ, we may replace W_1 and W_2 by the leading term $(m-1)\rho_2\bar{\omega}_2^2$. In the finite-Larmor-radius terms in $W_2 - W_1$, we replace $\bar{\omega}_{12}$ and $\bar{\omega}_{23}$ by $-\frac{1}{2}m\omega_2$. Finally, we assume region 2 to be thin, so that $r_{12} \approx r_{23}$ and $\epsilon = 2m\delta$, where

$$\delta \equiv (r_{23} - r_{12})/r_{12}. \quad (23)$$

With these approximations Eq. (22) becomes

$$(m-1)\rho_1\bar{\omega}_1^2 + (m+1)\rho_3\bar{\omega}_3^2 + \delta(m^2-1)\rho_2\bar{\omega}_2^2 - [\omega^2 - \gamma m^2(m^2-1)\omega_2](\rho_3 - \rho_1) = 0. \quad (24)$$

We have actually done a more careful job of ordering and have obtained additional small terms, but Eq. (24) contains all the essential features of the solution, and further refinement does not seem justified in view of the crudeness of the original model. Expanding Eq. (24) and defining $\alpha_i \equiv \rho_i/(\rho_1 + \rho_3)$, we obtain the following dispersion equation:

$$[1 + \delta\alpha_2(m^2-1)/m]\omega^2 - 2[(m-1)\alpha_1\omega_1 + (m+1)\alpha_3\omega_3 + \delta(m^2-1)\alpha_2\omega_2]\omega + m[(m-1)\alpha_1\omega_1^2 + (m+1)\alpha_3\omega_3^2 + \delta(m^2-1)\alpha_2\omega_2^2 + \gamma(m^2-1)\omega_2(\alpha_3 - \alpha_1)] = 0. \quad (25)$$

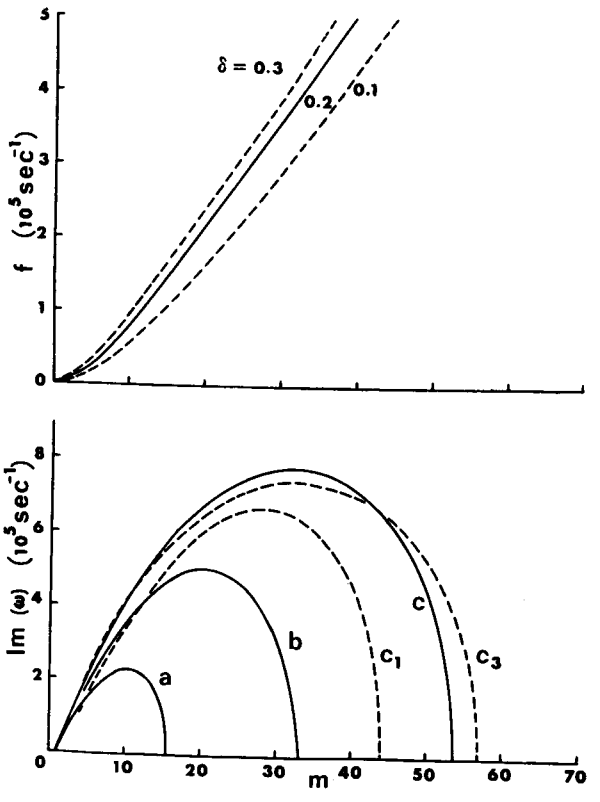

FIG. 15. The three-region solution for f and $\mathrm{Im}(\omega)$ as a function of m-number for $\alpha_2 = 0.5$, $\omega_2 = 10^5$, $\omega_3 = 2 \times 10^4$ sec^{-1}. Other parameters same as in FIG. 12. Solid curves: $\delta = 0.2$; dashed curves: $\delta = 0.1(c_1)$ and $0.3(c_3)$, with $\gamma(\alpha_1 - \alpha_2) = 1500$. Curves (a), (b), and (c) correspond approximately to $B = 2$, 3.3, and 5 kG, respectively.

Frequencies and growth rates computed from Eq. (25) are shown in Fig. 15. The parameters are the same as for Fig. 13, except that a middle layer of thickness $\delta = 0.2 \pm 0.1$ with rotation frequency $\omega_2 = 10^5$ sec^{-1} has been added. Note that the frequencies have been shifted to higher values by the $\delta\alpha_2\omega_2$ term; this is the expected Doppler shift. This term dominates over a finite-Larmor-radius term which we neglected; hence, the frequencies coincide for different values of γ. The γ term in Eq. (25) has a smaller stabilizing effect than it did in the two-region case. This is because the $\delta\alpha_2\omega_2^2$ term is dominant in the constant term of Eq. (25), and finite-Larmor-radius stabilization occurs only at very large m-numbers.

C. Discussion

What is the justification for using finite-Larmor-radius equations and then assuming that the density and electric field change discontinuously in a distance small compared with r_L? First, there is a precedent for this procedure in the solution of the hydrodynamic problem of two fluids—say, of wind blowing over water. The equations for an inviscid fluid are used in that case[2] to describe the interior of each fluid, where the relevant scale lengths are much larger than the collision mean free path λ_c. At the boundary, there is a layer of thickness of order λ_c in which viscosity must be taken into account. This layer is customarily neglected, and the matching of inviscid solutions is made with a jump condition. In the case of magnetoplasma, we replace λ_c with r_L and use the finite-Larmor-radius equations in the interior of each fluid, where the scale lengths are much larger than r_L. At the boundary, there is a layer of thickness of order r_L in which finite-Larmor-radius equations break down and higher-order terms in the ion orbit integrals should be taken into account. We neglect this layer and replace it with a jump condition. In both the hydrodynamic and the plasma cases this procedure is justified by reasonable agreement with experiment. In neither case does one expect the theory to be extremely accurate.

Second, the sharp-boundary model makes more sense when one considers exactly which finite-Larmor-radius effect has been retained. By assuming uniform ρ and E_0/r in the interior of each region, we have neglected both the diamagnetic drift and the finite-Larmor-radius correction to the ion $\mathbf{E} \times \mathbf{B}$ drift in equilibrium. At the interface, there is a diamagnetic current connected with the discontinuous jump in density. This does not give rise to the γ term we have retained; for if one redoes the calculation keeping diamagnetic effects but neglecting the finite Larmor radius by dropping the viscosity tensor, one would simply recover the hydrodynamic fluid result with the diamagnetic drift added to V_0. Hence, all finite-Larmor-radius effects in the equilibrium have been neglected; the γ term comes from the finite-Larmor-radius effect connected with the nonuniformity of the *perturbed* electric field. When the interface is rippled, an E field in the θ direction is created. The ions drift more slowly than the electrons in this nonuniform E field, and because of the jump in density at the interface a space charge arises. In accordance with a picture given by Chen,[7] this space charge causes a phase shift between the fluctuations in density and potential which slows down and eventually stops the instability. Thus, the finite-Larmor-radius effect has been retained only to predict the correct cutoff of wave growth at high m numbers in the two-region solution.

The physical interpretation of the three-region solution is considerably more complicated. Apparently, the Kelvin–Helmholtz effect is so large in

the presence of the high-velocity layer that finite-Larmor-radius stabilization can be neglected at small m numbers. The growth rate (Fig. 15) peaks at larger m numbers than are observed, and it would appear that the three-region solution does not predict this peak accurately. We believe that this is partly due to the approximations made in reducing Eq. (22) to a quadratic, and partly due to the inaccuracy of the sharp-boundary model. On the other hand, the frequencies (Fig. 15) are given quite accurately because they depend mainly on the $\mathbf{E}\times\mathbf{B}$ velocities in the three regions, weighted by the relative number of ions in each region.

We now return to the question of finite $k_\parallel$. The measurements of $k_\parallel$ shown in Fig. 6 are not entirely inconsistent with a standing wave with $\lambda_\parallel = 4L$. Such a wave with a node at the hot plate and a maximum at the cold plate would be consistent with the theory of end-plate damping.[8] Furthermore, this value of $\lambda_\parallel$ is small enough to put the experiment in the drift-excitation range of the resistive drift wave dispersion curve.[12] However, the drift effects are of the same order of magnitude as the finite-Larmor-radius effects, and we have seen that these effects are dominated by the Kelvin–Helmholtz effects in the three-region treatment. Thus, we have reason to believe that the $k_\parallel = 0$ theory is applicable to the experiment whether or not $\lambda_\parallel$ was as short as $4L$. The finite-$k_\parallel$ terms can easily be added to Eq. (1), but one would then lose the benefits of an analytic solution.

IV. COMPARISON OF THEORY WITH EXPERIMENT

The frequency and m number of the dominant mode has been measured under various conditions as regards magnetic field, plasma density, and aperture limiter configuration. In each case, the density and potential profiles were measured and approximated by step functions, as shown in Fig. 14. From these step functions, the theoretical frequency and growth rate was calculated from Eq. (25). The comparison of the calculated frequencies with the observed frequencies is shown in Fig. 16. The indicated errors arise mainly from the measurement of E_0 from the potential profiles. It is seen that the agreement is quite good, and much better than with any theory that does not take into account the nonuniform electric field. The calculated frequencies are generally somewhat higher than those measured. This is probably due to the neglect of the zero-order nonuniformity of E_0 in the middle region, an effect which would slow down the rotation of the plasma.

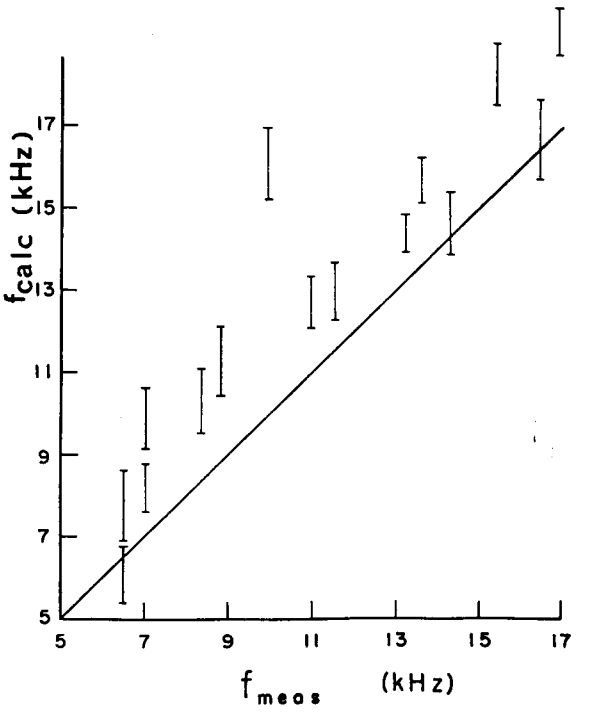

FIG. 16. Comparison of the measured frequencies with the frequencies calculated from the three-region solution and the measured profiles.

Figure 17 shows a comparison of the B dependence of the measured amplitude with that of the theoretical growth rate for the $m = 3$, 4, and 5 modes. The dashed lines are the *experimental* data of Fig. 10. The points are values of Im (ω) computed from Eq. (25) and the measured profiles. The agreement suggests that the saturation amplitude is not un-

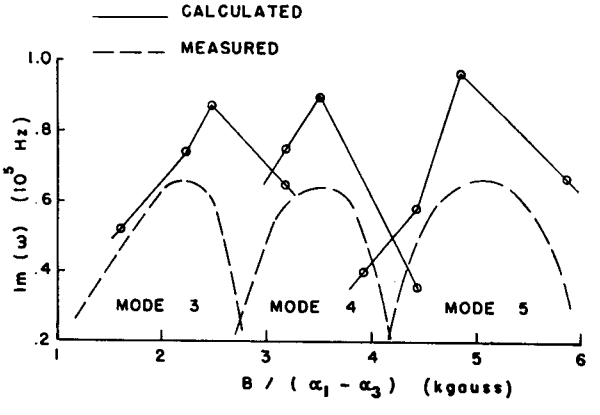

FIG. 17. The calculated growth rate and the measured wave amplitude as a function of $B/(\alpha_1 - \alpha_3)$, where $\alpha_1 - \alpha_3$ is the relative density change in going from the interior to the exterior region.

[12] F. F. Chen, Phys. Fluids 8, 1323 (1965).

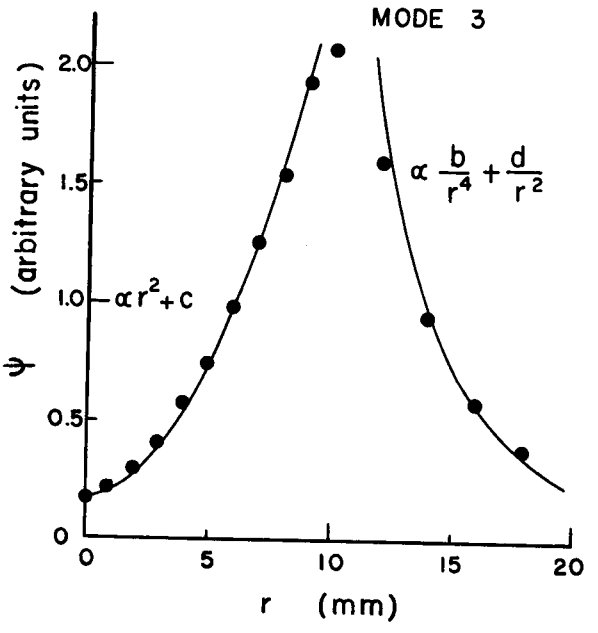

FIG. 18. Comparison of experimental (points) and theoretical (line) radial amplitude distributions for the $m = 3$ mode. The theoretical curve includes a small admixture of the $m = 1$ mode to account for the finite wave amplitude at $r = 0$.

related to the theoretical growth rate. Note that Im (ω) increases monotonically with B if the plasma profile is kept constant, as can be seen from Fig. 15. The fact that Im (ω) falls again at high B (for fixed m) is due to a change in the plasma profile. At large B, Fig. 15 would predict a large number of unstable modes. This is consistent with the broadening of the spectrum of Fig. 4 at high magnetic field.

Figure 18 shows the measured radial dependence of wave amplitude for the $m = 3$ mode. The theoretical curves are the interior and exterior eigenfunctions of Eq. (7). To account for the nonvanishing amplitude at $r = 0$, we have had to assume a small admixture of the $m = 1$ mode, which has constant amplitude at $r = 0$, as can be seen from Eq. (7). The good agreement between theory and experiment here gives credence to the validity of our step-function model, for, as we stated earlier, the results are sensitive to the form of the radial wavefunction.

V. SUMMARY AND RELATED WORK

We have shown that the "edge" oscillation observed in Q machines is a transverse Kelvin–Helmholtz instability adequately described by a $k_\parallel = 0$ theory of Rosenbluth and Simon.[9] Centrifugal and drift excitation of the oscillations have been shown to be unimportant in the experiment. Theory and experiment show reasonable agreement as regards wave frequency, B dependence of growth rate, and radial amplitude distribution.

Although we believe we have identified the instability, there is room for improvement both experimentally and theoretically. In particular, the theoretical calculations can be refined successively by (a) solving the entire quartic equation (22), (b) assuming more realistic forms for $\rho(r)$ and $E_0(r)$ in the various regions, (c) numerically integrating Eq. (1) without dividing the plasma into regions, (d) adding finite-$k_\parallel$ terms to Eq. (1), and (e) improving Eq. (1) by going to higher order in r_L/R.

We believe that this Kelvin–Helmholtz instability is responsible for oscillations above 5 kHz observed in early work in alkali plasmas and erroneously identified as drift waves. The original paper of D'Angelo and Motley[13] did not show a radial amplitude distribution, but subsequent papers by Buchel'nikova,[14] D'Angelo *et al.*,[15] Lashinsky,[16] and Hartman,[17] showed oscillation amplitudes that were definitely peaked at the radial boundary. Most of these results have been summarized by Hendel, Chu, and Politzer.[18] More recent experiments on drift waves[18–20] have been made with the recognition that the edge oscillation is a separate phenomenon.

An experiment similar to ours has been reported by Enriques, Levine, and Righetti.[21] The geometry of their experiment was somewhat cleaner than ours, but no theoretical explanation was given; the experimental results were similar. In the interior of an alkali plasma the radial E fields are relatviely weak, but their nonuniformity can affect the excitation of drift waves. This has been studied by Hartman and Munger[22] and by Chen and Rogers.[23] Many experiments in small Q machines are performed in weak magnetic fields ($\sim$ 1 kG). In such

[13] N. D'Angelo and R. W. Motley, Phys. Fluids **6**, 422 (1963).
[14] N. S. Buchel'nikova, Nucl. Fusion **4**, 165 (1964).
[15] N. D'Angelo, D. Eckhartt, G. Grieger, E. Guilino, and M. Hashmi, Phys. Rev. Letters **11**, 525 (1963).
[16] H. Lashinsky, in *Plasma Physics and Controlled Nuclear Fusion Research* (International Atomic Energy Agency, Vienna, 1966), Vol. I, p. 499.
[17] C. W. Hartman and R. H. Munger, in *Plasma Instabilities and Anomalous Transport* (University of Miami Press, Coral Gables, Florida, 1966), p. 149.
[18] H. W. Hendel, T. K. Chu, and P. A. Poltizer, Phys. Fluids **11**, 2426 (1968).
[19] F. F. Chen and D. Mosher, Phys. Rev. Letters **18**, 639 (1967).
[20] P. F. Little and C. R. Middleton, Nucl. Fusion Pt. 1, **9**, 67 (1969).
[21] L. Enriques, A. M. Levine, and G. B. Righetti, Plasma Phys. **10**, 641 (1968).
[22] C. W. Hartman and R. H. Munger, in *Proceedings of the Conference on Physics of Quiescent Plasmas* (Euratom–C.N.E.N., Frascati, Italy, 1967), Pt. I, p. 49.
[23] F. F. Chen and K. C. Rogers, Bull. Am. Phys. Soc., **13**, 1548 (1968).

experiments the large electric field at the edge can penetrate far into the plasma because of the large-ion Larmor radius, and the Kelvin–Helmholtz effects cannot be neglected. Particularly suspicious are reports of "drift waves" in single-ended Q machines such as ours. The ion lifetime in such devices is so short that drift waves generally do not have time to grow unless the excitation is aided by the centrifugal or Kelvin–Helmholtz effect.

Finally, we wish to point out that it is important to use shielded probes in Q machines, since probes must penetrate the region where these relatively high-frequency oscillations can exist.

ACKNOWLEDGMENTS

We are indebted to I. Mansfield for help with the construction and operation of the Q machine. One of us (G. K.) wishes to thank Dr. H. Hendel for valuable comments on his thesis.

This work was supported by the United States Air Force Office of Scientific Research under Grant No. 1093-67A.